

Article

Simultaneous Production of Aromatics and CO_x-Free Hydrogen via Methane Dehydroaromatization in Membrane Reactors: A Simulation Study

Feng Ye ¹, Shuanshi Fan ^{1,*}, Wenjun Li ², Yanhong Wang ¹, Xuemei Lang ¹, Jianli Zhang ³, Jing Li ^{1,4}
and Gang Li ^{1,4,*}

¹ School of Chemistry and Chemical Engineering, South China University of Technology, Guangzhou 510640, China

² Beijing Institute of Spacecraft System Engineering, Beijing 100086, China

³ State Key Laboratory of High-Efficiency Utilization of Coal and Green Chemical Engineering, College of Chemistry and Chemical Engineering, Ningxia University, Yinchuan 750021, China

⁴ South China University of Technology-Zhuhai Institute of Modern Industrial Innovation, Zhuhai 519175, China

* Correspondence: ssfan@scut.edu.cn (S.F.); fegli@scut.edu.cn (G.L.)

Abstract: As an alternative route for aromatics and hydrogen production, methane dehydroaromatization (MDA) is of significant academic and industrial interest due to the abundance of natural gas resources and the intensive demand for aromatics and CO_x-free hydrogen. In the present work, a simulation study on MDA in membrane reactors (MRs) was performed with the aim of co-producing aromatics and CO_x-free hydrogen with a highly improved efficiency. The effects of various parameters, including catalytic activity, membrane flux and selectivity, as well as the operating conditions on the MR performance were discussed with respect to methane conversion, hydrogen yield, and hydrogen purity. The results show that catalytic activity and membrane flux and selectivity have significant impacts on CH₄ conversion and H₂ yield, whereas H₂ purity is mainly dominated by membrane selectivity. A highly improved MDA is confirmed to be feasible at a relatively low temperature and a high feed pressure because of the hydrogen extraction effect. To further improve MDA in MRs by intensifying H₂ extraction, a simple configuration combining a fixed-bed reactor (FBR) and an MR together is proposed for MDA, which demonstrates good potential for the high-efficiency co-production of aromatics and CO_x-free hydrogen.

Keywords: methane dehydroaromatization; membrane reactor; CO_x-free hydrogen; aromatics; hydrogen separation



Citation: Ye, F.; Fan, S.; Li, W.; Wang, Y.; Lang, X.; Zhang, J.; Li, J.; Li, G. Simultaneous Production of Aromatics and CO_x-Free Hydrogen via Methane Dehydroaromatization in Membrane Reactors: A Simulation Study. *Membranes* **2022**, *12*, 1175. <https://doi.org/10.3390/membranes12121175>

Academic Editors: Jie Shen, Zongyao Zhou and Sheng Zhou

Received: 8 November 2022

Accepted: 19 November 2022

Published: 22 November 2022

Publisher's Note: MDPI stays neutral with regard to jurisdictional claims in published maps and institutional affiliations.



Copyright: © 2022 by the authors. Licensee MDPI, Basel, Switzerland. This article is an open access article distributed under the terms and conditions of the Creative Commons Attribution (CC BY) license (<https://creativecommons.org/licenses/by/4.0/>).

1. Introduction

Natural gas is the most abundant and cleanest energy carrier among fossil resources; thus, the conversion of methane instead of petroleum and coal into liquid fuels and high-value-added chemicals has been highly desirable in the chemical industry [1–6], particularly with the recent boom in the exploitation of unconventional shale gas [7–11] and natural gas hydrate [12,13] resources and with increasing concerns over environmental issues worldwide. Currently, the catalytic conversion of methane to important products, for instance, methanol [14] and olefins [15], is technologically dominated by an indirect route, which involves multistep reactions, and the highly energy-intensive intermediate step for syngas production, either by reforming or by partial oxidation, is generally inevitable, which results in a complicated process with a high production cost and a poor atom economy [16]. Therefore, direct conversion of methane to liquid fuels and chemicals without the syngas production intermediate step is of significant importance for practical applications.

In particular, a direct route, i.e., methane dehydroaromatization (MDA) ($\text{CH}_4 \rightleftharpoons \frac{1}{6}\text{C}_6\text{H}_6 + \frac{3}{2}\text{H}_2$) under nonoxidative conditions, has gained significant interest

for methane utilization after a pioneering study by Wang et al. [17]. Compared with the conventional aromatic production process using petroleum as the feedstock, the MDA process has been widely accepted as an attractive alternative to produce aromatics with a better sustainability. On the other hand, it is noteworthy that the MDA process can simultaneously generate substantial CO_x -free hydrogen, which can be directly used as the fuel for polymer electrolyte membrane fuel cells (PEMFCs) with neither the removal of CO, which is a poison to the Pt catalyst, nor the emission of CO_2 , which is mainly responsible for the greenhouse effect. Therefore, CO_x -free hydrogen produced from MDA demonstrates significant advantages against the conventional methane steam reforming process, i.e., the main route for current hydrogen production with an intensive energy consumption and massive emissions [18,19], in PEMFC applications. Currently, one of the major obstacles to the industrial implementation of the MDA process is its relatively low conversion because MDA is significantly limited by thermodynamic equilibrium. To achieve an acceptable conversion, MDA must be conducted at very high temperatures (≥ 700 °C) [20–24]; unfortunately, this results in very rapid catalyst deactivation due to the serious coking effect. Thus far, how to simultaneously maintain a high conversion and high catalytic stability for MDA remains a great challenge for industrial applications.

Membrane reactors (MRs), which integrate both separation and catalytic processes into a compact single unit, are promising for enhancing the conversion and/or enabling a lower reaction temperature for thermodynamically limited endothermic reactions because of the equilibrium shift effect. Considering the above advantages against conventional fixed-bed reactors (FBRs), MRs are extremely attractive for high-temperature MDA reactions, and various types of MRs have been successfully developed in an attempt to improve MDA performance [25–33]. Among them, most studies focus on Pd and its alloy MRs for MDA application because of its exclusive permeation for hydrogen; however, these Pd-based membranes are very expensive and prone to degradation at high temperatures [26]. Although highly hydrogen-permselective dense ceramic membranes with an excellent stability have been examined as an alternative for MDA application [30,31], the flux of these membranes is too low. On the other hand, in addition to hydrogen-permselective MRs, dense oxygen-permeable ceramic MRs, which allow for finely tuned oxygen distribution in the feed, were also employed for MDA [32,33], and an improved catalytic performance was observed due to the favorable thermodynamics of MDA under oxidative conditions. However, the addition of oxygen to the feed using oxygen-permeable ceramic membranes should be controlled very carefully; otherwise, overoxidation is prone to occur, which results in an extremely low selectivity for MDA. Furthermore, because the generation of CO under oxidative conditions is inevitable, hydrogen produced from oxygen-permeable MRs must be subjected to further purification before use in PEMFCs, which greatly impairs the economic and technical feasibility of the produced hydrogen for PEMFC applications because the separation of CO from hydrogen to an extremely low concentration is both costly and challenging.

Considering the high flux and high selectivity, as well as the excellent thermal stability, porous inorganic membranes, such as zeolite and amorphous silica, are good candidates for MDA applications. Unfortunately, to the best of our knowledge, no porous MRs have been reported for MDA, and details regarding how such factors as the catalytic activity, membrane performance and operating conditions affect the MR performance of MDA in terms of CH_4 conversion, H_2 yield and H_2 purity are still not well understood. In this study, a simulation study of MDA in porous hydrogen-permselective MRs is conducted for the simultaneous production of aromatics and CO_x -free hydrogen, and insights into the above membrane intensification process would offer important inspiration for developing high-performance porous MRs for practical MDA applications.

2. Modeling

The mathematical model for MDA in concurrent configuration MRs was developed based on the following assumptions: (1) the reactor is isothermal and operates under a

steady state, (2) both the feed and permeate streams in the reactor are plug flows and a catalytic reaction only occurs in the feed stream, (3) concentration polarization effects are negligible, and (4) there are no pressure drops in the MR. A schematic model for the simulation study of MRs is shown in Figure 1.

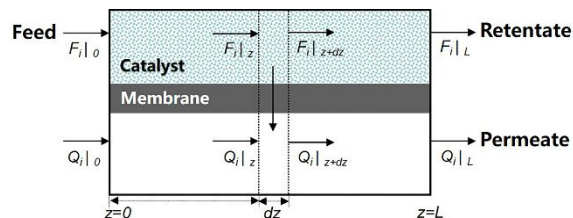


Figure 1. Schematic model for the membrane reactor simulation.

The molar flow rate of component i in the MR can be expressed as follows [34,35]:

Feed side

$$\frac{dF_i}{dz} = v_i R w_{cat} - s P_i (x_i p_h - y_i p_l) \tag{1}$$

Permeate side

$$\frac{dQ_i}{dz} = s P_i (x_i p_h - y_i p_l) \tag{2}$$

where F_i and Q_i are molar flow rates of component i in the feed and permeate streams, and x_i and y_i are denoted as their corresponding molar fractions, respectively, p_h and p_l are the pressures of the feed and permeate streams, respectively, z is the axial position along the membrane, v_i is the stoichiometric number of component i , P_i indicates the permeance of component i through the membrane, w_{cat} and s indicate the catalyst weight and membrane area per membrane unit length, respectively, and R is the reaction rate of MDA based on the following global reaction equation:



It is believed that a highly stable and selective catalyst for MDA can be expected by carefully tuning the properties of the support and metal species [36–38]. Therefore, side reactions in MDA are not considered in the present modeling for simplification in order to evaluate the potential of benzene production in MRs. With the assistance of the dimensionless parameters of the Damköhler number (Da), permeation number (θ), reaction rate (R^*), pressure (p_r), permeance ($\alpha_{H_2/i}$), and axial position (ζ) defined in Equations (4)–(9):

$$Da = R^{max} W_{cat} / F_{CH_4,0} \tag{4}$$

$$\theta = P_{H_2} s L p_h / F_{CH_4,0} \tag{5}$$

$$R^* = R / R^{max} \tag{6}$$

$$p_r = p_l / p_h \tag{7}$$

$$\alpha_{H_2/i} = P_{H_2} / P_i \tag{8}$$

$$\zeta = z / L \tag{9}$$

Equations (1) and (2) can be further expressed as dimensionless forms, as shown in Equations (10) and (11), respectively.

Feed side

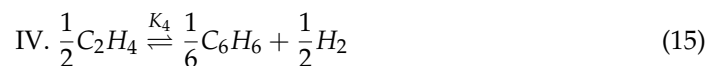
$$\frac{df_i}{d\zeta} = v_i R^* Da - \frac{\theta (x_i - y_i p_r)}{\alpha_{H_2/i}} \tag{10}$$

Permeate side

$$\frac{dq_i}{d\zeta} = \frac{\theta(x_i - y_i p_r)}{\alpha_{H_2/i}} \tag{11}$$

where f_i and q_i are the dimensionless flow rates normalized by the CH₄ feed flow rate for component i in the feed and permeate streams, respectively, ζ is the axial position of the MR normalized by the membrane length, θ is defined as the permeation number that corresponds to H₂ flux through the membrane normalized by the CH₄ feed low rate, $\alpha_{H_2/i}$ is the permeance ratio of H₂ to component i , p_r is the pressure ratio of the permeate stream to the feed stream, R^* is the ratio of the reaction rate R to the maximum reaction rate R^{max} based on the inlet feed composition, Da is the Damköhler number, which is defined as the ratio of the product of the maximum reaction rate R^{max} and the total catalyst weight of the membrane module W_{cat} to the CH₄ feed flow rate, and Da indicates the effect of the catalyst and the feed flow rate on the catalytic performance, which can be used as a measure of the catalytic activity. The higher Da is, the closer the reaction is to equilibrium.

According to a simple single-site mechanism [39], the global reaction of MDA (Equation (3)) consists of the following series of elementary steps:



where * indicates the active site of the catalyst, and step III is obtained by merging the CH₂ dimerization and C₂H₄ desorption steps in Equations (16) and (17):



Step II is considered to be the rate-determining step in MDA, yielding a reaction rate expression for the global reaction in Equation (18) [39].

$$R = k_2 \frac{P_{CH_4} - \frac{1}{K_p} P_{C_6H_6}^{1/6} P_{H_2}^{3/2}}{1 + K_1 P_{CH_4} + \frac{K_3}{K_4} P_{C_6H_6}^{1/6} P_{H_2}^{1/2}} \tag{18}$$

where

$$K_4 = \exp\left(-\frac{\Delta G_4}{R_g T}\right) \left(p^\ominus\right)^{\frac{1}{6}} \tag{19}$$

$$K_p = \exp\left(-\frac{\Delta G}{R_g T}\right) \left(p^\ominus\right)^{\frac{2}{3}} \tag{20}$$

p^\ominus is the standard pressure, P_{CH_4} , $P_{C_6H_6}$ and P_{H_2} are the partial pressures of CH₄, C₆H₆, and H₂, respectively, ΔG and ΔG_4 are the Gibbs free energies of the global (Equation (1)) and step IV (Equation (15)) reactions, respectively, k_2 is the reaction rate constant of step II, and K_1 , K_3 , K_4 and K_p are equilibrium constants for steps I, III, IV and the global reaction, respectively. For a 0.5%Ru-3%Mo/ZSM-5 catalyst, the reaction rate and equilibrium constants (K_1 , K_3 , k_2) are shown in Table 1 according to Iliuta et al. [39], which were adopted in the present work for the simulation study.

Table 1. Reaction rate and equilibrium constants used in the present simulation.

Temperature (K)	k_2 (mol g _{cat} ⁻¹ h ⁻¹ bar ⁻¹)	K_1 (bar ⁻¹)	K_3 (bar ^{-1/2})
873	0.00717	2.877	2.359
898	0.0102	2.197	2.870
923	0.014	1.675	3.020
948	0.019	1.280	3.185
973	0.025	1.029	3.300

The simulation study of MDA in concurrent MRs was performed at temperatures of 873–973 K, with porous H₂-permselective membranes, showing H₂/CH₄ selectivities in the range of 10–∞, under feed and permeate pressures of 100–1000 and 5 kPa, respectively. Because both CH₄ and C₆H₆ are much larger than H₂ in terms of molecular size, they are assumed to permeate through the defects of H₂-permselective membranes based on a Knudsen diffusion mechanism; therefore, the selectivity of CH₄ to C₆H₆ in the MR is fixed to the Knudsen selectivity in the simulation. Because benzene is a condensable product that is easily separated and collected on both retentate and permeate sides of the MR, the yield of benzene in the MR is defined based on the product obtained in both retentate and permeate streams, and the effect of the presence of benzene on the final H₂ purity can be negligible. On the other hand, both H₂ yield and H₂ purity is defined based on only the permeate side, because purified H₂ is highly desirable. Therefore, the CH₄ conversion (X_{CH_4}), benzene yield ($Y_{C_6H_6}$), H₂ yield (Y_{H_2}), and H₂ purity (C_{H_2}) obtained in the MRs are defined as follows:

$$X_{CH_4} = \frac{F_{CH_4,0} - F_{CH_4,L} - Q_{CH_4,L}}{F_{CH_4,0}} \quad (21)$$

$$Y_{C_6H_6} = \frac{6F_{C_6H_6,L} + 6Q_{C_6H_6,L}}{F_{CH_4,0}} \quad (22)$$

$$Y_{H_2} = \frac{2Q_{H_2,L}}{3F_{CH_4,0}} \quad (23)$$

$$C_{H_2} = \frac{Q_{H_2,L}}{Q_{CH_4,L} + Q_{H_2,L}} \quad (24)$$

For FBRs, the CH₄ conversion, benzene yield, H₂ yield and H₂ purity are defined in Equations (25)–(28):

$$X_{CH_4} = \frac{F_{CH_4,0} - F_{CH_4,L}}{F_{CH_4,0}} \quad (25)$$

$$Y_{C_6H_6} = \frac{6F_{C_6H_6,L}}{F_{CH_4,0}} \quad (26)$$

$$Y_{H_2} = \frac{2F_{H_2,L}}{3F_{CH_4,0}} \quad (27)$$

$$C_{H_2} = \frac{F_{H_2,L}}{F_{CH_4,L} + F_{H_2,L}} \quad (28)$$

3. Results and Discussion

3.1. Thermodynamic Analysis and Model Validation

Figure 2 shows the equilibrium conversion of CH₄ in MDA under different temperatures and feed pressures. The equilibrium conversion of CH₄ is quite low, particularly under a low temperature and a high pressure. The above calculation confirms that MDA is significantly thermodynamically unfavorable. Although CH₄ conversion in MDA can be improved by increasing the reaction temperature, catalyst deactivation is reportedly even faster due to the more serious coking effect at a higher temperature [40]. Therefore,

to strike a balance between CH_4 conversion and catalytic stability, MDA is generally conducted at $700\text{ }^\circ\text{C}$ and at atmospheric pressure [21–23], which corresponds to an equilibrium conversion of approximately 12% due to the significant thermodynamic limitation. The above results demonstrate that there is significant potential to use H_2 -permselective MRs for highly enhanced MDA because the equilibrium of MDA can be efficiently shifted to the product side after selective H_2 extraction.

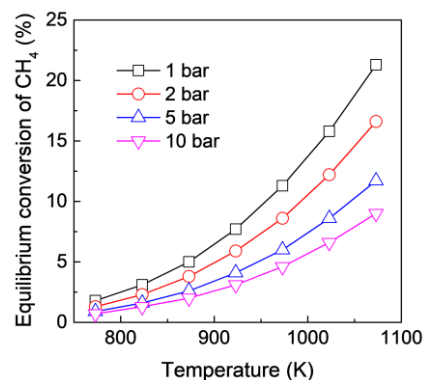


Figure 2. Equilibrium conversion of CH_4 in MDA under different temperatures and pressures.

To validate the proposed model for the simulation study of MDA in MRs, we first calculated the CH_4 conversion based on the present model and previously reported experimental parameters [39] using the same cylindrical reactor without H_2 extraction under various operating conditions. As shown in Figure 3, both the theoretically predicted and experimentally obtained CH_4 conversions showed an excellent agreement, which verifies the feasibility of the proposed model for the simulation study of MDA. Unfortunately, further verification cannot be conducted by applying H_2 extraction to MRs because Pd-based membranes are prone to poison in the presence of hydrocarbons at high temperatures, and the actual H_2 permeation performance of the membrane reactor, which is reportedly significantly different compared with that obtained during the H_2 permeation test [28], is currently not yet available during MDA.

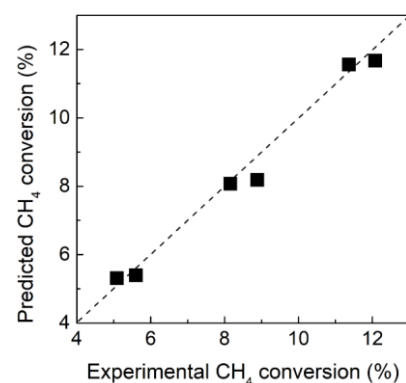


Figure 3. Comparison of experimentally obtained and theoretically predicted CH_4 conversions in the MR without H_2 extraction.

3.2. Effect of Catalysts on the MR Performance

Figure 4 shows the effect of the Damköhler number on CH_4 conversion, H_2 yield, and H_2 purity as a function of the permeation number for MDA in the MR. When the catalytic activity of the MR is relatively low, for instance, $Da = 0.2$ and 0.5 , both CH_4 conversion and H_2 yield obtained in the MR gradually increased with an increasing permeation number, which could be ascribed to the improved equilibrium shift effect, since H_2 extraction from the MR is enhanced. For MR with a relatively active catalyst ($Da \geq 1$), the improvement in the CH_4 conversion and H_2 yield is more remarkable due to the enhanced driving force

for H₂ extraction. However, both the CH₄ conversion and H₂ yield show a maximum as the permeation number increases, which could be mainly attributed to the adverse effect of CH₄ permeation through the membrane because the amount of CH₄ permeation through the membrane becomes remarkable at high *Da* values and permeation numbers. Similar trends were also previously observed for various dehydrogenation reactions in H₂-permselective MRs [34,35]. On the other hand, the H₂ purity in the permeate stream always decreases with an increasing permeation number, regardless of the values of *Da*, which mainly results from the enhanced CH₄ permeation through the membrane at a high permeation number. However, for a given permeation number, H₂ purity increases as *Da* increases because CH₄ conversion is improved and the permeation of CH₄ through the membrane becomes slower. The above results demonstrate that an active catalyst is necessary for the effective enhancement of MDA in an MR with respect to CH₄ conversion, H₂ yield and H₂ purity.

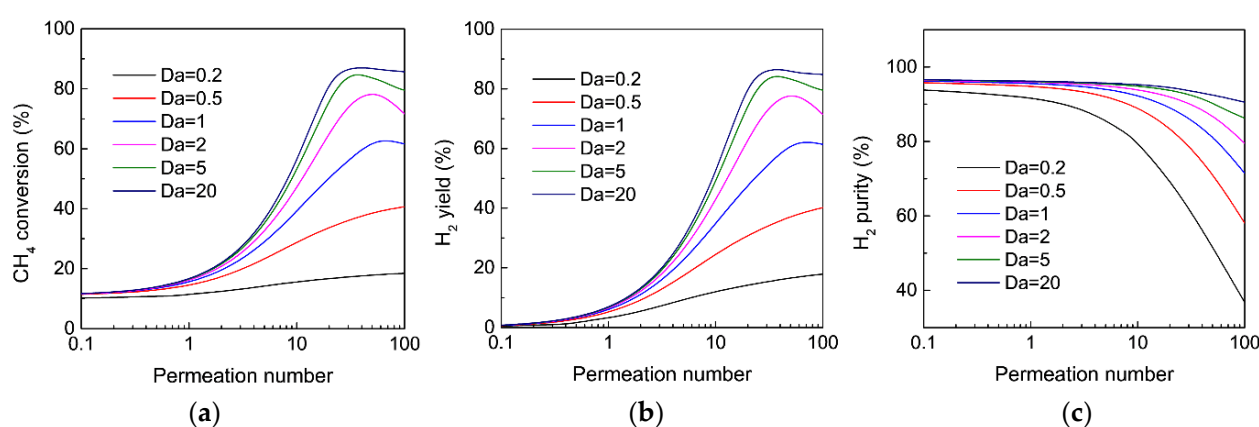


Figure 4. Effect of the Damköhler number on (a) CH₄ conversion, (b) H₂ yield, and (c) H₂ purity as a function of permeation number for MDA in the MR. (Simulation conditions: $T = 973$ K, $\alpha_{H_2/CH_4} = 200$, $\alpha_{CH_4/C_6H_6} =$ Knudsen selectivity, $p_h = 1$ bar, $p_l = 0.05$ bar).

3.3. Effect of Membranes on the MR Performance

Figure 5 shows the effect of H₂/CH₄ selectivity of the membrane on CH₄ conversion, H₂ yield, and H₂ purity as a function of permeation number for MDA in the MR. As the permeation number increases from 0.1 to 100, both the CH₄ conversion and H₂ yield in porous MRs with a given H₂/CH₄ selectivity initially increase and then subsequently decrease, resulting in a maximum. This is because the equilibrium shift effect after H₂ extraction that contributes to the improved CH₄ conversion and yield is dominative at a relatively low permeation number, whereas the effect of CH₄ permeation from the feed to the permeate side that lowers the CH₄ conversion and yield becomes very important at a high permeation number. The maximal CH₄ conversion and H₂ yield are effectively enhanced as the H₂/CH₄ selectivity of the MR is increased from 10 to 500 because the leakage of CH₄ from the feed to permeate sides can be significantly reduced with a highly H₂-selective membrane. Note that the MR shows a low degree of improvement in CH₄ conversion and H₂ yield at a low permeation number, even though the membrane selectivity is extremely high. This is because only a very limited amount of H₂ is extracted from the reactor at a relatively low permeation number. Therefore, a remarkable improvement is achieved only for MR with both an acceptable H₂ flux and selectivity.

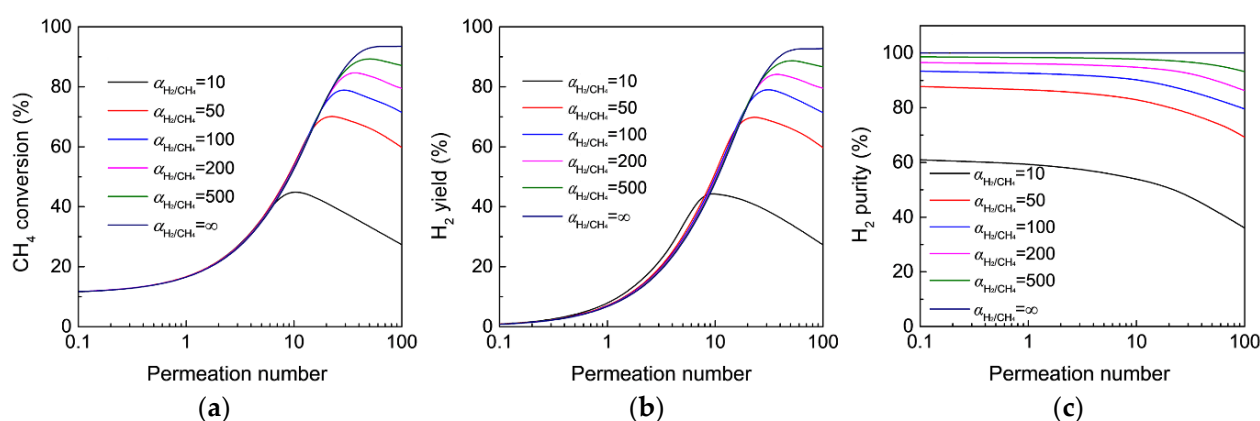


Figure 5. Effect of H_2/CH_4 selectivity on (a) CH_4 conversion, (b) H_2 yield, and (c) H_2 purity as a function of permeation number for MDA in the membrane reactor. (Simulation conditions: $T = 973$ K, $Da = 5$, $\alpha_{CH_4/C_6H_6} =$ Knudsen selectivity, $p_h = 1$ bar, $p_l = 0.05$ bar).

Considering the excellent H_2 separation performance of Pd-based membranes, MDA in MRs should be effectively improved after H_2 extraction according to the present and previously reported theoretical simulations [41,42]. However, experimental investigations [25,26,28] have demonstrated that Pd-based MRs show only a very limited enhancement for MDA compared with FBRs under the same operating conditions. We believe that the remarkable difference between the theoretical prediction and the experimental results is most likely attributed to the significantly decreased H_2 permeation flux of Pd-based membranes during MDA because Pd-based membranes are reportedly poisoned in the presence of hydrocarbons at high temperatures [43], which significantly hinder H_2 permeation by blocking Pd sites on the membrane surface from adsorbing and dissociating H_2 molecules. Recently, Natesakhawat et al. [28] compared the H_2 permeation performance of a tubular Pd membrane in 10% H_2/N_2 and 10% H_2/CH_4 mixtures at 700 °C to study the effect of CH_4 on the Pd membrane performance. The Pd membrane in a later system lost up to 75% of its H_2 permeability, which confirms the occurrence of serious CH_4 poisoning for the Pd membrane. Moreover, the reduction of H_2 permeability of Pd membranes was reportedly even much more noticeable during MDA [28]. The above simulation results confirm that the poor catalytic performance of Pd-based MRs in experimental investigations most likely results from the severe degradation of H_2 permeation flux during MDA.

Importantly, it is worth noting that the porous MR with a H_2/CH_4 selectivity of 200 shows almost the same MDA performance in terms of the CH_4 conversion and H_2 yield compared with those of the dense Pd-based MR with an infinite H_2/CH_4 selectivity under the same permeation number ranging from 0.1 to 30, and both the maximal CH_4 conversion and H_2 yield exceed 80%, which demonstrates a significant potential for highly enhanced MDA in the porous MRs. Although dense Pd membranes show an exclusive permeation for H_2 , taking their relatively lower flux during MDA and the high cost into consideration, porous MRs with an acceptable cost and H_2/CH_4 selectivity (>200) but a much higher H_2 permeance ($>10^{-6}$ mol Pa $^{-1}$ m $^{-2}$ s $^{-1}$) free of CH_4 poisoning, such as amorphous silica membranes [44–46], would be preferable for MDA in practical applications in terms of the CH_4 conversion and H_2 yield.

The H_2 purity obtained in the MR can be significantly enhanced as the membrane selectivity increases, and the effect of the permeation number seems to have much less of an impact on the H_2 purity, particularly for the MR with a H_2 selectivity over 200. The above results demonstrate that both the CH_4 conversion and H_2 yield obtained in the MR are greatly affected by both the catalytic activity and membrane performance, while the H_2 purity is mainly dominated by the membrane selectivity. In this regard, dense Pd membranes with exclusive H_2 permeation are preferable when the H_2 purity is a priority for MDA in the MR. Therefore, the selection of membrane materials should be carefully

considered according to the objective MR performance in terms of the CH_4 conversion, H_2 yield, and H_2 purity.

3.4. Effect of Operating Conditions on the MR Performance

Thermodynamically, the coking reaction is much more favorable than MDA at a high temperature and leads to catalyst deactivation during MDA. To reduce the effect of coking on the catalytic stability, it is preferable to perform MDA under a relatively low temperature, which would impair the CH_4 conversion for MDA in the conventional FBR. However, MR allows for the possibility that MDA is conducted at a lower temperature, whereas the CH_4 conversion remains high because of the equilibrium shift effect after H_2 extraction. Figure 6 shows the effect of the reaction temperature on the CH_4 conversion, H_2 yield, and H_2 purity as a function of the permeation number for MDA in the MR. As expected, for a given permeation number, although CH_4 conversion, H_2 yield, and H_2 purity all decrease with a decreasing reaction temperature because MDA is thermodynamically unfavorable at a low temperature, the MR performance greatly surpasses that obtained in the conventional FBR under the same reaction temperature, and the improvement is still extremely remarkable, even under 873 K if the MR is highly permeable. The above results demonstrate the significant importance of intensifying the MR performance for MDA by improving H_2 permeance via reducing the membrane thickness. This is particularly important for MDA operated under a lower reaction temperature because the H_2 partial pressure difference across the membrane is lower for H_2 permeation. Recent progress has demonstrated that emerging two-dimensional-material membranes [47] constructed by 2D nanosheets with few atomic thickness layers show both a high flux and high selectivity, which would be a future candidate for the development of high-performance MRs for MDA.

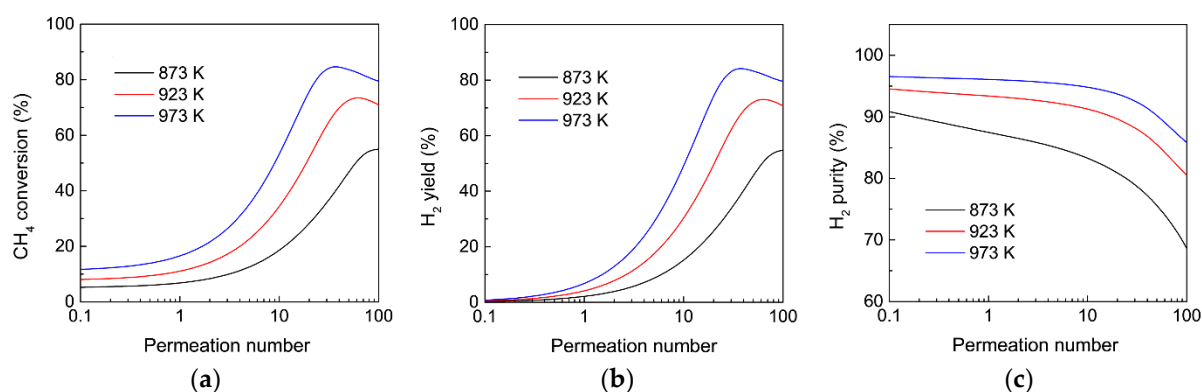


Figure 6. Effect of the reaction temperature on (a) CH_4 conversion, (b) H_2 yield, and (c) H_2 purity as a function of the permeation number for MDA in the membrane reactor. (Simulation conditions: $Da = 5$, $\alpha_{\text{H}_2/\text{CH}_4} = 200$, $\alpha_{\text{CH}_4/\text{C}_6\text{H}_6} = \text{Knudsen selectivity}$, $p_h = 1 \text{ bar}$, $p_l = 0.05 \text{ bar}$).

On the other hand, although a high feed pressure is not favorable for MDA in an FBR according to the equilibrium shift by Le Chatelier's principle, as also confirmed in the aforementioned calculation (Figure 2), the effect of the feed pressure on MDA in the MR is more complicated because a high pressure also favors H_2 permeation through the membrane, which is believed to boost MDA in MRs from the viewpoint of an equilibrium shift due to the enhancing H_2 extraction. Therefore, whether a high feed pressure benefits MDA in MRs depends on the equilibrium shift effect caused by both H_2 extraction and the feed pressure. However, how the feed pressure affects MDA in MRs remains unclear. Figures 7 and 8 show the effect of the feed pressure on CH_4 conversion, H_2 yield, and H_2 purity as a function of permeation number for MDA in the MR at 873 and 973 K, respectively. For the same permeation number with a relatively low value, the MR shows a decreased CH_4 conversion with an increasing feed pressure, regardless of the reaction temperature, because the final CH_4 conversion is largely affected by the equilibrium shift effect by high feed pressures. However, when the permeation number is larger than 10,

compared with MDA in the MR under atmospheric pressure, the MR shows an enhanced CH_4 conversion along with an improved H_2 yield and purity in a pressurized system, although the high pressure is unfavorable for MDA in FBRs, which could be ascribed to the significant contribution of the equilibrium shift effect by enhanced H_2 extraction at high feed pressures. It should be noted that the MR performance could again deteriorate at much higher pressures because the effect of feed pressure on the MR performance becomes more remarkable. For instance, the CH_4 conversion at a feed pressure of 10 bar is lower than that obtained at atmospheric pressure at 873 K, even though the MR is highly permeable (Figure 8). Therefore, there is an optimal feed pressure to maximize the MDA performance in MRs, and the value highly depends on the specific reaction conditions used, such as temperature and catalyst.

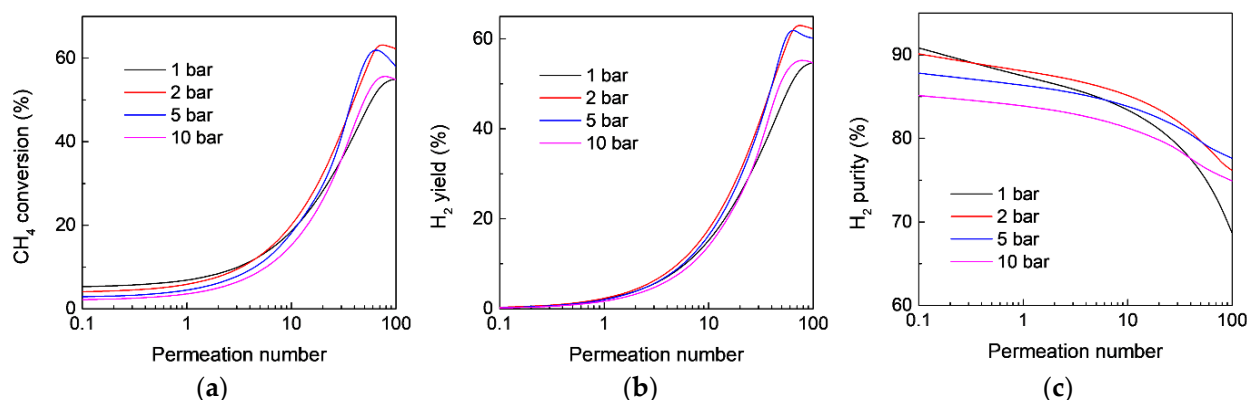


Figure 7. Effect of the feed pressure on (a) CH_4 conversion, (b) H_2 yield, and (c) H_2 purity as a function of the permeation number for MDA in the membrane reactor. (Simulation conditions: $T = 873$ K, $Da = 5$, $\alpha_{\text{H}_2/\text{CH}_4} = 200$, $\alpha_{\text{CH}_4/\text{C}_6\text{H}_6} = \text{Knudsen selectivity}$, $p_l = 0.05$ bar).

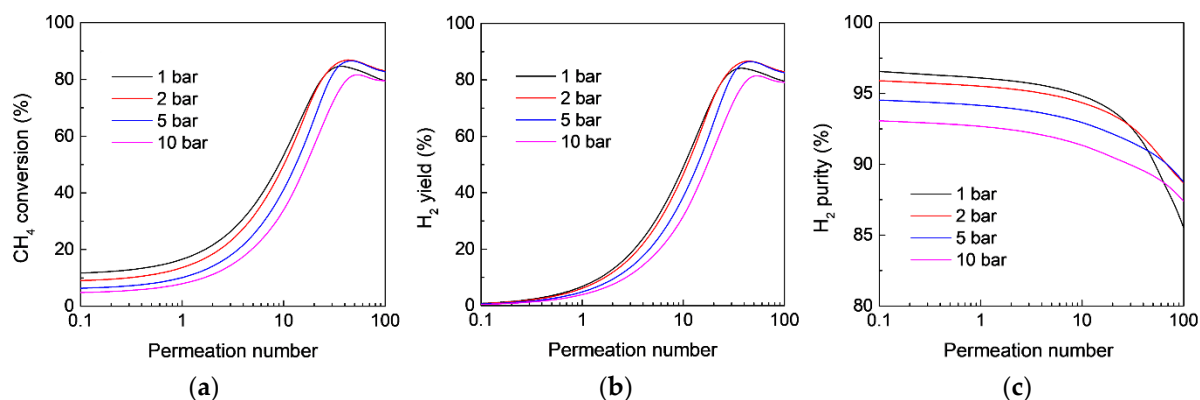


Figure 8. Effect of CH_4 feed pressure on (a) CH_4 conversion, (b) H_2 yield, and (c) H_2 purity as a function of the permeation number for MDA in the membrane reactor. (Simulation conditions: $T = 973$ K, $Da = 5$; $\alpha_{\text{H}_2/\text{CH}_4} = 200$, $\alpha_{\text{CH}_4/\text{C}_6\text{H}_6} = \text{Knudsen selectivity}$, $p_l = 0.05$ bar).

3.5. Integration of an FBR and an MR for Enhanced MDA

The enhancement of the MR performance is significantly affected by the amount of extracted H_2 during the reaction, and thus a high membrane packing density is highly desirable for practical MDA applications. Hollow fiber MRs are generally preferable when taking the very high packing density into account [48]. However, one of the major obstacles to the practical use of hollow fiber MRs is the relatively low catalyst loading capacity, which generally results in a poor performance of MRs due to the relatively low catalytic activity, as confirmed in Figure 4. This is because the H_2 partial pressure across the membrane, which is the driving force for H_2 permeation, is too low to extract sufficient H_2 from the MR. Consequently, H_2 permeation in hollow fiber MRs should be further intensified to

more efficiently promote the MDA performance. To achieve a higher MDA performance, a facile configuration that integrates a fixed-bed reactor (FBR) and an MR is suggested for MDA in which the FBR functions as a pre-reactor. For comparison, the performance of MDA in a single conventional FBR and a single MR are studied under identical operating conditions. The schematic reactor configurations are shown in Figure 9.

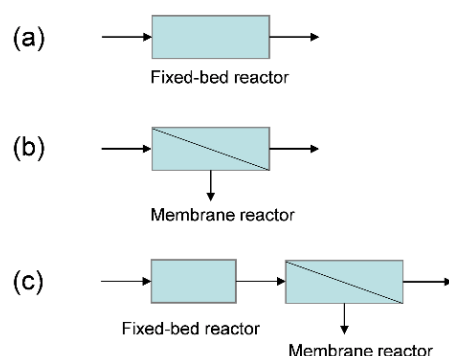


Figure 9. Different reactor configurations used for MDA. (a) Fixed-bed reactor; (b) membrane reactor; (c) integration of a fixed-bed reactor and a membrane reactor.

Figure 10 shows the effect of reactor configurations on the CH_4 conversion, H_2 yield, and H_2 purity for MDA in the MR under different feed pressures. For a comparison, catalyst loading in the FBR (Figure 9a) and MRs (Figure 9b,c) are fixed at the same amount, while the CH_4 conversion in the FBR (Figure 9c) is assumed to achieve equilibrium under atmospheric pressure because a high catalyst loading in the FBR is practically feasible. For the single conventional FBR (Figure 9a), the CH_4 conversion, H_2 yield and H_2 purity are 10.7, 10.7 and 10.5%, respectively, at a feed pressure of 1 bar, and all of these values decrease with an increasing feed pressure, which can be ascribed to the equilibrium shift of MDA to the backward side at high feed pressures. However, the MDA performance is much enhanced in the single MR, particularly under a high feed pressure, although a pressurized system is unfavorable for MDA in an FBR. As the feed pressure increases from 1 to 2 and 3 bar, the CH_4 conversion gradually increases from 23.3 to 32.7 and 37.6%, with the H_2 yield increasing from 21.3 to 32.1 and 37.3%, and the H_2 purity decreasing from 74.3 to 66.6 and 60.1%, respectively. This remarkable improvement in the MDA can be ascribed to the equilibrium shift effect of the MR after H_2 extraction, where a higher feed pressure effectively promotes H_2 extraction due to the higher H_2 partial pressure difference across the membrane, as evidenced by the axial profiles of the normalized H_2 partial pressure in the MR under different feed pressures in Figure 11a. The above result demonstrates that the MR performance under present pressurized conditions is largely affected by the equilibrium shift effect caused by H_2 extraction, rather than by a high pressure. When an FBR is coupled with the MR (Figure 9c), after completion of the reaction in the FBR, the H_2 partial pressure is quite high at the inlet of the MR, which would facilitate H_2 extraction during the subsequent MR due to the increased driving force for H_2 permeation. As expected, CH_4 conversion in the MR is further improved to 31.3% at a feed pressure of 1 bar with the assistance of an FBR, and a higher feed pressure in the MR even improves the CH_4 conversion to a higher degree (41.2 and 46.2% at 2 and 3 bar, respectively). The corresponding H_2 yield also increases from 29.4 to 40.7 and 46.1%, whereas the H_2 purity decreases from 74.3 to 66.6 and 60.1 at 1, 2 and 3 bar, respectively. Previously, an improved conversion was also observed for methylcyclohexane dehydrogenation in an MR when a FBR was coupled [49]. With the assistance of FBR as a pre-reactor, the exceptional MDA performance in the MR was primarily ascribed to the enhanced H_2 extraction. As confirmed by the axial profiles of the normalized H_2 partial pressure for MDA in the MR in Figure 11b, the employment of a pre-reactor indeed increases the H_2 partial pressure difference across the membrane, particularly near the inlet zone of the MR. This effect is even more effective under pressurized systems, which further promotes the equilibrium shift of MDA to the

forward side and results in a much higher CH₄ conversion and H₂ yield and purity than those obtained in the single FBR and the single MR.

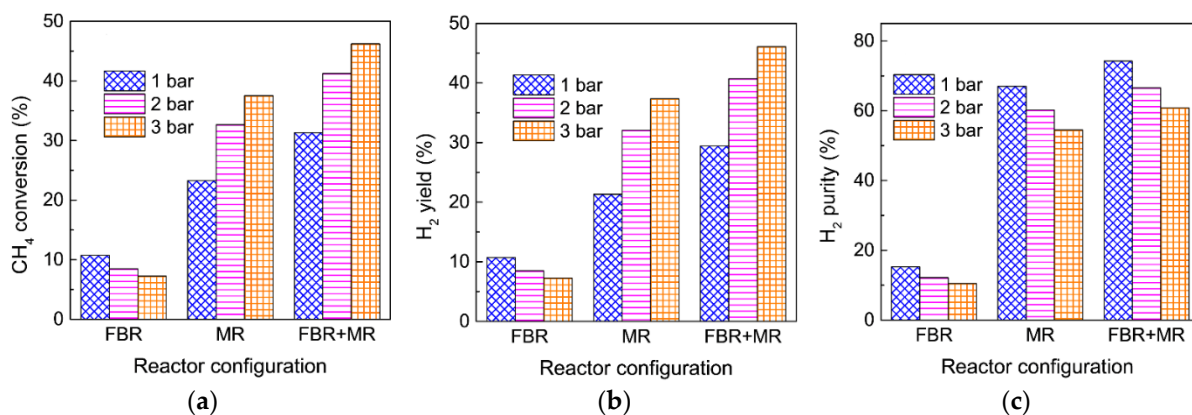


Figure 10. Effect of reactor configurations on (a) CH₄ conversion, (b) H₂ yield, and (c) H₂ purity for MDA in the membrane reactor with different CH₄ feed pressures. (Simulation conditions: Temperature = 973 K, catalyst amount = 0.15 g, CH₄ feed = 6.59×10^{-3} mol h⁻¹, H₂ permeance = 72 mol m⁻² h⁻¹ bar⁻¹, membrane length = 0.4 m, membrane diameter = 2.5×10^{-3} m, $\alpha_{H_2/CH_4} = 200$, α_{CH_4/C_6H_6} = Knudsen selectivity, $p_l = 0.05$ bar, and $p_h = 1, 2$ and 3 bar).

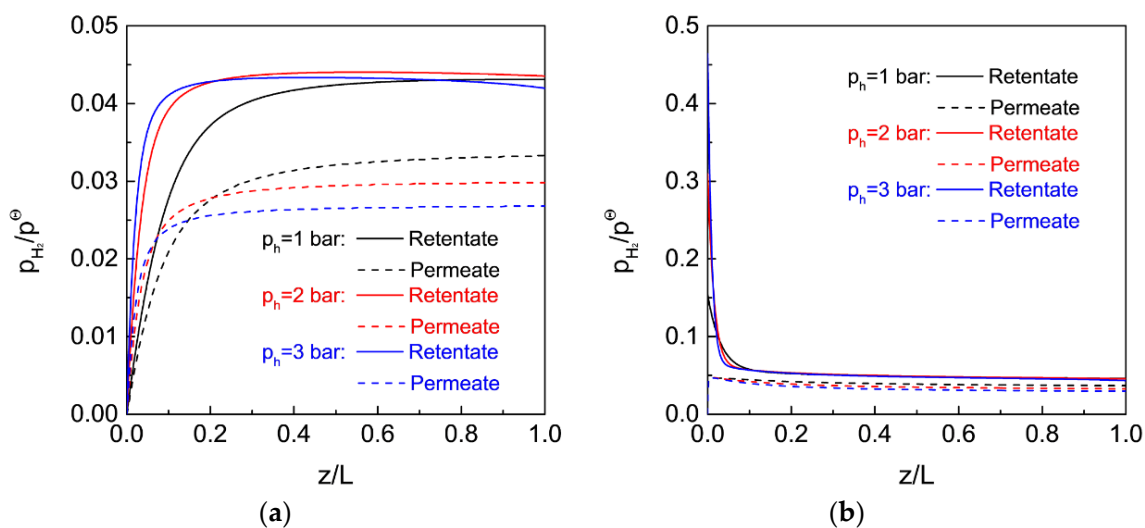


Figure 11. Axial profiles of H₂ partial pressure normalized by the standard pressure for MDA in the membrane reactor under different feed pressures (a) with and (b) without the assistance of a pre-reactor. (Simulation conditions: Temperature = 973 K, catalyst amount = 0.15 g, CH₄ feed = 6.59×10^{-3} mol h⁻¹, H₂ permeance = 72 mol m⁻² h⁻¹ bar⁻¹, membrane length = 0.4 m, membrane diameter = 2.5×10^{-3} m, $\alpha_{H_2/CH_4} = 200$, α_{CH_4/C_6H_6} = Knudsen selectivity, $p_l = 0.05$ bar, and $p_h = 1, 2$ and 3 bar).

Considering the effectively enhanced H₂ extraction, the proposed simple reactor configuration that combines an FBR and an MR is superior to both the conventional single FBR and the single MR in terms of the CH₄ conversion, H₂ yield and H₂ purity. In addition, it should be noted that MDA is endothermic; therefore, heat transfer to the catalyst bed must be fast enough to maintain a constant temperature in the reactor. The new reactor configuration consisting of two parts allows for sectional heating for MDA, which again benefits MDA for simultaneous large-scale production of aromatics and CO_x-free H₂ in industrial applications under isothermal conditions.

4. Conclusions

A dimensionless mathematical model was formulated and verified for a simulation study on methane dehydroaromatization in H₂-permselective MRs for the simultaneous production of aromatics and CO_x-free H₂. The simulation results showed that the improvement in the CH₄ conversion and H₂ yield in the MR is strongly influenced by the catalytic activity and membrane flux and selectivity, whereas H₂ purity is mainly determined by the membrane selectivity. Compared with dense Pd-based membranes, porous membranes, such as amorphous silica, with a H₂/CH₄ selectivity of several hundred are highly preferable for MDA with respect to the both CH₄ conversion and H₂ yield due to the high H₂ permeance and the absence of CH₄ poisoning. Operating conditions, including the reaction temperature and pressure, also exert important impacts on the MR performance. A low temperature generally results in a decrease in the MDA performance due to unfavorable thermodynamics, but a significantly higher performance, compared with that of conventional FBRs, can still be achieved in MRs due to the equilibrium shift effect after H₂ extraction. Therefore, MRs have great potential to lower the reaction temperature and thus reduce the coking on the catalyst for MDA. A pressurized system is confirmed to further improve MDA in the MR under certain conditions due to the enhanced H₂ extraction, although a pressurized system is unfavorable for MDA in FBRs. Finally, a simple configuration that combines an FBR and an MR is proposed for MDA, which demonstrates a much better performance in terms of the CH₄ conversion, H₂ yield, and H₂ purity compared with both the single FBR and single MR due to the intensified H₂ extraction. This simple and effective configuration shows a great potential for the simultaneous production of aromatics and CO_x-free H₂ with a high efficiency for practical applications.

Author Contributions: Conceptualization, G.L.; investigation, F.Y.; writing—original draft preparation, F.Y.; writing—review and editing, S.F., W.L., Y.W., X.L., J.Z. and G.L.; project administration, J.Z.; funding acquisition, J.L. and G.L. All authors have read and agreed to the published version of the manuscript.

Funding: This research was funded by the National Natural Science Foundation of China, grant number U1662137; the Zhuhai Industry-University-Research Cooperation and Basic & Applied Basic Research Project, grant number ZH22017003210078PWC; and the Foundation of State Key Laboratory of High-Efficiency Utilization of Coal and Green Chemical Engineering, grant number 2021-K40.

Institutional Review Board Statement: Not applicable.

Data Availability Statement: Not applicable.

Conflicts of Interest: The authors declare no conflict of interest.

Nomenclature

Da	Damköhler number, dimensionless
f	dimensionless feed-side flow rate, dimensionless
F	feed-side molar flow rate, mol h ⁻¹
C	purity of hydrogen, dimensionless
k	reaction rate constant, mol g _{cat} ⁻¹ h ⁻¹ bar ⁻¹
k_2	reaction rate constant, mol g _{cat} ⁻¹ h ⁻¹ bar ⁻¹
K_1	equilibrium constant, bar ⁻¹
K_3	equilibrium constant, bar ^{-1/2}
K_4	equilibrium constant, bar ^{1/6}
K_p	equilibrium constant, bar ^{2/3}
L	membrane reactor length, m
p	partial pressure, bar
p^\ominus	standard pressure, bar
p_h	feed-side pressure, bar
p_l	permeate-side pressure, bar
p_r	pressure ratio, dimensionless

P	gas permeance, mol m ⁻² h ⁻¹ bar ⁻¹
q	dimensionless permeate-side flow rate, dimensionless
Q	permeate-side molar flow rate, mol h ⁻¹
R	reaction rate, mol g _{cat} ⁻¹ h ⁻¹
R_g	ideal gas constant, J mol ⁻¹ K ⁻¹
R_{max}	maximum reaction rate, mol g _{cat} ⁻¹ h ⁻¹
R^*	dimensionless reaction rate, dimensionless
s	membrane area per unit membrane axial length, m ² m ⁻¹
T	absolute temperature, K
w_{cat}	catalyst weight per unit membrane axial length, g _{cat} m ⁻¹
W_{cat}	catalyst weigh of the membrane module, g
x	feed-side mole fraction, dimensionless
X	conversion, dimensionless
y	permeate-side mole fraction, dimensionless
Y	yield, dimensionless
z	axial coordinate, m
Greek letters	
α	permeance ratio, dimensionless
θ	permeation number, dimensionless
ν	stoichiometric coefficient, dimensionless
ζ	dimensionless axial coordinate, dimensionless
ΔG	Gibbs free energy, J mol ⁻¹
ΔG_4	Gibbs free energy, J mol ⁻¹
Subscripts	
0	inlet of the membrane reactor
i	component
L	outlet of the membrane reactor

References

- Schwach, P.; Pan, X.; Bao, X. Direct conversion of methane to value-added chemicals over heterogeneous catalysts: Challenges and prospects. *Chem. Rev.* **2017**, *117*, 8497–8520. [[CrossRef](#)] [[PubMed](#)]
- Wang, B.; Albarracín-Suazo, S.; Pagán-Torres, Y.; Nikolla, E. Advances in methane conversion processes. *Catal. Today* **2017**, *285*, 147–158. [[CrossRef](#)]
- Guo, X.; Fang, G.; Li, G.; Ma, H.; Fan, H.; Yu, L.; Ma, C.; Wu, X.; Deng, D.; Wei, M.; et al. Direct, nonoxidative conversion of methane to ethylene, aromatics, and hydrogen. *Science* **2014**, *344*, 616–619. [[CrossRef](#)] [[PubMed](#)]
- Jin, Z.; Wang, L.; Zuidema, E.; Mondal, K.; Zhang, M.; Zhang, J.; Wang, C.; Meng, X.; Yang, H.; Mesters, C.; et al. Hydrophobic zeolite modification for in situ peroxide formation in methane oxidation to methanol. *Science* **2020**, *367*, 193–197. [[CrossRef](#)] [[PubMed](#)]
- Shan, J.; Li, M.; Allard, L.F.; Lee, S.; Flytzani-Stephanopoulos, M. Mild oxidation of methane to methanol or acetic acid on supported isolated rhodium catalysts. *Nature* **2017**, *551*, 605–608. [[CrossRef](#)]
- Spivey, J.J.; Hutchings, G. Catalytic aromatization of methane. *Chem. Soc. Rev.* **2014**, *43*, 792–803. [[CrossRef](#)] [[PubMed](#)]
- Schnoor, J.L. Shale gas and hydrofracturing. *Environ. Sci. Technol.* **2012**, *46*, 4686. [[CrossRef](#)]
- Dong, D.; Wang, Y.; Li, X.; Zou, C.; Guan, Q.; Zhang, C.; Huang, J.; Wang, S.; Wang, H.; Liu, H.; et al. Breakthrough and prospect of shale gas exploration and development in China. *Nat. Gas Ind. B* **2016**, *3*, 12–26. [[CrossRef](#)]
- Chang, Y.; Liu, X.; Christie, P. Emerging shale gas revolution in China. *Environ. Sci. Technol.* **2012**, *46*, 12281–12282. [[CrossRef](#)]
- Striolo, A.; Cole, D.R. Understanding shale gas: Recent progress and remaining challenges. *Energy Fuels* **2017**, *31*, 10300–10310. [[CrossRef](#)]
- Salygin, V.; Guliev, I.; Chernysheva, N.; Sokolova, E.; Toropova, N.; Egorova, L. Global shale revolution: Successes, challenge, and prospects. *Sustainability* **2019**, *11*, 1627. [[CrossRef](#)]
- Li, J.-F.; Ye, J.-L.; Qin, X.-W.; Qiu, H.-J.; Wu, N.-Y.; Lu, H.-L.; Xie, W.-W.; Lu, J.-A.; Peng, F.; Xu, Z.-Q.; et al. The first offshore natural gas hydrate production test in South China Sea. *China Geol.* **2018**, *1*, 5–16. [[CrossRef](#)]
- Ye, J.-L.; Qin, X.-W.; Xie, W.-W.; Lu, H.-L.; Ma, B.-J.; Qiu, H.-J.; Liang, J.-Q.; Lu, J.-A.; Kuang, Z.-G.; Lu, C.; et al. The second natural gas hydrate production test in the South China Sea. *China Geol.* **2020**, *3*, 197–209. [[CrossRef](#)]
- Blumberg, T.; Tsatsaronis, G.; Morosuk, T. On the economics of methanol production from natural gas. *Fuel* **2019**, *256*, 115824. [[CrossRef](#)]
- Tian, P.; Wei, Y.; Ye, M.; Liu, Z. Methanol to olefins (MTO): From fundamentals to commercialization. *ACS Catal.* **2015**, *5*, 1922–1938. [[CrossRef](#)]

16. Mevawala, C.; Bai, X.; Kotamreddy, G.; Bhattacharyya, D.; Hu, J. Multiscale modeling of a direct nonoxidative methane dehydroaromatization reactor with a validated model for catalyst deactivation. *Ind. Eng. Chem. Res.* **2021**, *60*, 4903–4918. [[CrossRef](#)]
17. Wang, L.; Tao, L.; Xie, M.; Xu, G.; Huang, J.; Xu, Y. Dehydrogenation and aromatization of methane under non-oxidizing conditions. *Catal. Lett.* **1993**, *21*, 35–41. [[CrossRef](#)]
18. Alhamdani, Y.A.; Hassim, M.H.; Ng, R.T.L.; Hurme, M. The estimation of fugitive gas emissions from hydrogen production by natural gas steam reforming. *Int. J. Hydrog. Energy* **2017**, *42*, 9342–9351. [[CrossRef](#)]
19. Chen, B.; Liao, Z.; Wang, J.; Yu, H.; Yang, Y. Exergy analysis and CO₂ emission evaluation for steam methane reforming. *Int. J. Hydrog. Energy* **2012**, *37*, 3191–3200. [[CrossRef](#)]
20. Kosinov, N.; Uslamin, E.A.; Coumans, F.J.A.G.; Wijkema, A.S.G.; Rohling, R.Y.; Hensen, E.J.M. Structure and evolution of confined carbon species during methane dehydroaromatization over Mo/ZSM-5. *ACS Catal.* **2018**, *8*, 8459–8467. [[CrossRef](#)] [[PubMed](#)]
21. Thakur, R.; Hoffman, M.; Vahi dMohammadi, A.; Smith, J.; Chi, M.; Tatarchuk, B.; Beidaghi, M.; Carrero, C.A. Multilayered two-dimensional V₂CT_x MXene for methane dehydroaromatization. *ChemCatChem* **2020**, *12*, 3639–3643. [[CrossRef](#)]
22. Vollmer, I.; Li, G.; Yarulina, I.; Kosinov, N.; Hensen, E.J.; Houben, K.; Mance, D.; Baldus, M.; Gascon, J.; Kapteijn, F. Relevance of the Mo-precursor state in H-ZSM-5 for methane dehydroaromatization. *Catal. Sci. Technol.* **2018**, *8*, 916–922. [[CrossRef](#)]
23. Liu, Y.; Zhao, M.; Cheng, L.; Yang, J.; Liu, L.; Wang, J.; Yin, D.; Lu, J.; Zhang, Y. Facile synthesis and its high catalytic performance of hierarchical ZSM-5 zeolite from economical bulk silicon oxides. *Microporous Mesoporous Mater.* **2018**, *260*, 116–124. [[CrossRef](#)]
24. Çağlayan, M.; Paioni, A.L.; Abou-Hamad, E.; Shterk, G.; Pustovarenko, A.; Baldus, M.; Chowdhury, A.D.; Gascon, J. Initial carbon–carbon bond formation during the early stages of methane dehydroaromatization. *Angew. Chem. Int. Ed.* **2020**, *59*, 16741–16746. [[CrossRef](#)]
25. Rival, O.; Grandjean, B.P.A.; Guy, C.; Sayari, A.; Larachi, F. Oxygen-free methane aromatization in a catalytic membrane reactor. *Ind. Eng. Chem. Res.* **2001**, *40*, 2212–2219. [[CrossRef](#)]
26. Iliuta, M.C.; Grandjean, B.P.A.; Larachi, F. Methane nonoxidative aromatization over Ru-Mo/HZSM-5 at temperature up to 973 K in a palladium-silver/stainless membrane reactor. *Ind. Eng. Chem. Res.* **2003**, *42*, 323–330. [[CrossRef](#)]
27. Kee, B.; Karakaya, C.; Zhu, H.; DeCaluwe, S.; Kee, R.J. The influence of hydrogen-permeable membranes and pressure on methane dehydroaromatization in packed-bed catalytic reactor. *Ind. Eng. Chem. Res.* **2017**, *56*, 3551–3559. [[CrossRef](#)]
28. Natesakhawat, S.; Means, N.C.; Howard, B.H.; Smith, M.; Abdelsayed, V.; Baltrus, J.P.; Cheng, Y.; Lekse, J.W.; Link, D.; Morreale, B.D. Improved benzene production from methane dehydroaromatization over Mo/HZSM-5 catalysts via hydrogen-permselective palladium membrane reactors. *Catal. Sci. Technol.* **2015**, *5*, 5023–5036. [[CrossRef](#)]
29. Kinage, A.K.; Ohnishi, R.; Ichikawa, M. Marked enhancement of the methane dehydrocondensation toward benzene using effective Pd catalytic membrane reactor with Mo/ZSM-5. *Catal. Lett.* **2003**, *88*, 199–202. [[CrossRef](#)]
30. Xue, J.; Chen, Y.; Wei, Y.; Feldhoff, A.; Wang, H.; Caro, J. Gas to liquids: Natural gas conversion to aromatic fuels and chemicals in a hydrogen-permeable ceramic hollow fiber membrane reactor. *ACS Catal.* **2016**, *6*, 2448–2451. [[CrossRef](#)]
31. Sakbodin, M.; Wu, Y.; Oh, S.C.; Wachsmann, E.D.; Liu, D. Hydrogen-permeable tubular membrane reactor: Promoting conversion and product selectivity for non-oxidative activation of methane over an Fe@SiO₂ catalyst. *Angew. Chem.* **2016**, *128*, 16383–16386. [[CrossRef](#)]
32. Cao, Z.; Jiang, H.; Luo, H.; Baumann, S.; Meulenber, W.A.; Assmann, J.; Mleczko, L.; Liu, Y.; Caro, J. Natural gas to fuels and chemicals: Improved methane aromatization in an oxygen-permeable membrane reactor. *Angew. Chem. Int. Ed.* **2013**, *52*, 13794–13797. [[CrossRef](#)] [[PubMed](#)]
33. Morejudo, S.H.; Zanón, R.; Escolástico, S.; Yuste-Tirados, I.; Malerød-Fjeld, H.; Vestre, P.K.; Coors, W.G.; Martínez, A.; Norby, T.; Serra, J.M.; et al. Direct conversion of methane to aromatics in a catalytic co-ionic membrane reactor. *Science* **2016**, *353*, 563–566. [[CrossRef](#)] [[PubMed](#)]
34. Tsuru, T.; Yamaguchi, K.; Yoshioka, T.; Asaeda, M. Methane steam reforming by microporous catalytic membrane reactors. *AIChE J.* **2004**, *50*, 2794–2805. [[CrossRef](#)]
35. Li, G.; Kanezashi, M.; Yoshioka, T.; Tsuru, T. Ammonia decomposition in catalytic membrane reactors: Simulation and experimental studies. *AIChE J.* **2013**, *59*, 168–179. [[CrossRef](#)]
36. Ma, D.; Lu, Y.; Su, L.; Xu, Z.; Tian, Z.; Xu, Y.; Lin, L.; Bao, X. Remarkable improvement on the methane aromatization reaction: A highly selective and coking-resistant catalyst. *J. Phys. Chem. B* **2002**, *106*, 8524–8530. [[CrossRef](#)]
37. Wang, N.; Dong, X.; Liu, L.; Cai, D.; Cheng, Q.; Wang, J.; Hou, Y.; Emwas, A.-H.; Gascon, J.; Han, Y. Probing the catalytic active sites of Mo/HZSM-5 and their deactivation during methane dehydroaromatization. *Cell Rep. Phys. Sci.* **2021**, *2*, 100309. [[CrossRef](#)]
38. Knonov, S.V.; Dubray, F.; Clatworthy, E.B.; Kouvatias, C.; Gilson, J.-P.; Dath, J.-P.; Minoux, D.; Aquino, C.; Valtchev, V.; Moldovan, S.; et al. Novel strategy for the synthesis of ultra-stable single-site Mo-ZSM-5 zeolite nanocrystals. *Angew. Chem. Int. Ed.* **2020**, *59*, 2–10.
39. Iliuta, M.C.; Iliuta, I.; Grandjean, B.P.A.; Larachi, F. Kinetics of methane nonoxidative aromatization over Ru–Mo/HZSM-5 catalyst. *Ind. Eng. Chem. Res.* **2003**, *42*, 3203–3209. [[CrossRef](#)]
40. Kosinov, N.; Hensen, E.J.M. Reactivity, selectivity, and stability of zeolite-based catalysts for methane dehydroaromatization. *Adv. Mater.* **2020**, *32*, 2002565. [[CrossRef](#)]

41. Wang, H.; Wang, B.; Qi, X.; Wang, J.; Yang, R.; Li, D.; Hu, X. Innovative non-oxidative methane dehydroaromatization via solar membrane reactor. *Energy* **2021**, *216*, 119265. [[CrossRef](#)]
42. Borry III, R.W.; Lu, E.C.; Kim, Y.-H.; Iglesia, E. Non-oxidative catalytic conversion of methane with continuous hydrogen removal. *Stud. Surf. Sci. Catal.* **1998**, *119*, 403–410.
43. Jung, S.H.; Kusakabe, K.; Morooka, S.; Kim, S.-D. Effects of co-existing hydrocarbons on hydrogen permeation through a palladium membrane. *J. Membr. Sci.* **2000**, *170*, 53–60. [[CrossRef](#)]
44. Akamatsu, K.; Suzuki, M.; Nakao, A.; Nakao, S. Development of hydrogen-selective dimethoxydimethylsilane-derived silica membranes with thin active separation layer by chemical vapor deposition. *J. Membr. Sci.* **2019**, *580*, 268–274. [[CrossRef](#)]
45. Kanezashi, M.; Asaeda, M. Hydrogen permeation characteristics and stability of Ni-doped silica membranes in steam at high temperature. *J. Membr. Sci.* **2006**, *271*, 86–93. [[CrossRef](#)]
46. Kageyama, N.; Takagaki, A.; Sugawara, T.; Kikuchi, R.; Oyama, S.T. Synthesis and characterization of a silica-alumina composite membrane and its application in a membrane reactor. *Sep. Purif. Technol.* **2018**, *195*, 437–445. [[CrossRef](#)]
47. Cheng, L.; Liu, G.; Zhao, J.; Jin, W. Two-dimensional-material membranes: Manipulating the transport pathway for molecular separation. *Acc. Mater. Res.* **2021**, *2*, 114–128. [[CrossRef](#)]
48. Pati, S.; Ashok, J.; Dewangan, N.; Chen, T.; Kawi, S. Ultra-thin (~1 μm) Pd–Cu membrane reactor for coupling CO₂ hydrogenation and propane dehydrogenation applications. *J. Membr. Sci.* **2020**, *595*, 117496. [[CrossRef](#)]
49. Li, G.; Yada, K.; Kanezashi, M.; Yoshioka, T.; Tsuru, T. Methylcyclohexane dehydrogenation in catalytic membrane reactors for efficient hydrogen production. *Ind. Eng. Chem. Res.* **2013**, *52*, 13325–13332. [[CrossRef](#)]